

3. Tamaki N, Kawamoto M, Yonekura Y, et al. Assessment of fatty acid metabolism using I-123 branched fatty acid: comparison with positron emission tomography. *Ann Nucl Med* 1993;7:S41-S47.
4. Saito S, Yasuda T, Gold HK, et al. Differentiation of regional perfusion and fatty acid uptake in zones of myocardial injury. *Nucl Med Commun* 1991;12:663-675.
5. Geeter FD, Franken PR, Knapp FF Jr, et al. Relationship between blood flow and fatty acid metabolism in subacute myocardial infarction: a study by means of ^{99m}Tc-sestamibi and ¹²³I-methyl-iodo-phenyl pentadecanoic acid. *Eur J Nucl Med* 1994;21:283-291.
6. Franken PR, Geeter FD, Dendale P, et al. Abnormal free fatty acid uptake in subacute myocardial infarction after coronary thrombolysis: correlation with wall motion and inotropic reserve. *J Nucl Med* 1994;35:1758-1765.
7. Knapp FF Jr, Franken P, Kropp J. Cardiac SPECT with iodine-123-labeled fatty acids: evaluation of myocardial viability with BMIPP. *J Nucl Med* 1995;36:1022-1030.
8. Gibbons RJ, Verani MS, Behrenbeck T, et al. Feasibility of tomographic ^{99m}Tc-hexakis-2-methoxy-2-methylpropyl-isonitrile imaging for the assessment of myocardial area at risk and the effect of treatment in acute myocardial infarction. *Circulation* 1989;80:1277-1286.
9. Gibbons RJ, Christian TF, Hopfenspirger M, et al. Myocardial at risk and infarct size after thrombolytic therapy for acute myocardial infarction: implications for the design of randomized trials of acute intervention. *J Am Coll Cardiol* 1994;24:616-623.
10. Christian TF, Schwartz RS, Gibbons RJ. Determinants of infarct size in reperfusion therapy for acute myocardial infarction. *Circulation* 1992;86:81-90.
11. O'Connor MK, Hammell T, Gibbons RJ. In vitro validation of a simple tomographic technique for estimation of percentage myocardium at risk using methoxyisobutyl isonitrile technetium-99m (sestamibi). *Eur J Nucl Med* 1990;17:69-76.
12. Dudczak R, Schmoliner R, Angelberger P, et al. Structurally modified fatty acids: clinical potential as tracers of metabolism. *Eur J Nucl Med* 1986;12:S45-S48.
13. Sandler H, Dodge HT. The use of single plane angiocardiology for the measurement of left ventricular volume in man. *Am Heart J* 1968;75:325-334.
14. Sheehan FH, Schofer J, Mathey DG, et al. Measurement of regional wall motion from biplane contrast ventriculograms: a comparison of the 30 degree right anterior oblique and 60 degree left anterior oblique projections in patients with acute myocardial infarction. *Circulation* 1986;74:796-804.
15. Sheehan FH, Schmidt WG, Bolson E. Influence of coronary arterial thrombus location on left ventricular function in acute myocardial infarction. *Am J Cardiol* 1990;66:16-21.
16. Christian TF, O'Connor MK, Hopfenspirger MR, et al. Comparison of reinjection thallium 201 and resting technetium-99m sestamibi tomographic images for the quantification of infarct size after acute myocardial infarction. *J Nucl Cardiol* 1994;1:17-28.
17. O'Connor MK, Gibbons RJ, Juni JE, et al. Quantitative myocardial SPECT for infarct sizing: feasibility of a multicenter trial evaluated using a cardiac phantom. *J Nucl Med* 1995;36:1130-1136.
18. Reimer KA, Jennings RB, Cobb FR, et al. Animal models for protecting ischemic myocardium: results of the NHLBI cooperative study: comparison of unconscious and conscious dog models. *Circ Res* 1985;56:651-665.
19. Feiring AJ, Johnson MR, Kioschos JM, et al. The importance of the determination of the myocardial area at risk in the evaluation of the outcome of acute myocardial infarction in patients. *Circulation* 1987;75:980-987.
20. Ito H, Tomooka T, Sakai N, et al. Time course of functional improvement in stunned myocardium in risk area in patients with reperfused anterior infarction. *Circulation* 1993;87:355-362.
21. Nanto S, Masuyama T, Lim YJ, et al. Demonstration of functional border zone with myocardial contrast echocardiography in human hearts: simultaneous analysis of myocardial perfusion and wall motion abnormalities. *Circulation* 1993;88:447-453.
22. Ahrens PJ, Sheehan FH, Dahl J, et al. Extension of hypokinesia into angiographically perfused myocardium in patients with acute infarction. *J Am Coll Cardiol* 1993;22:1010-1015.
23. Kropp J, Juergans M, Glaenger KP, et al. Evaluation of ischemia and myocardial viability in patients with coronary artery disease (CAD) with iodine-123 labeled 15-(p-iodophenyl)-3-R,S-methylpentadecanoic acid (BMIPP). *Ann Nucl Med* 1993;7:93-100.
24. Yamamichi Y, Kusuoka H, Morishita K, et al. Metabolism of iodine-123-BMIPP in perfused rat hearts. *J Nucl Med* 1995;36:1043-1050.
25. Weinstein H, Reinhardt CP, Marcel R, et al. Myocardial redistribution of BMIPP [Abstract]. *Circulation* 1995;92:1-789.
26. Takeishi Y, Chiba J, Abe S, et al. Heterogeneous myocardial distribution of iodine-123 15-(p-iodophenyl)-3-R,S-methylpentadecanoic acid (BMIPP) in patients with hypertrophic cardiomyopathy. *Eur J Nucl Med* 1992;19:775-782.
27. Okada RD. Kinetics of thallium-201 in reperfused canine myocardium after coronary artery occlusion. *J Am Coll Cardiol* 1984;3:1245-1251.
28. Liu P, Burns R. Easy come, easy go: time to pause and put thallium reverse redistribution in perspective. *J Nucl Med* 1993;34:1692-1694.
29. Sinusas AJ, Trautman KA, Bergin JD, et al. Quantification of area at risk during coronary occlusion and degree of myocardial salvage after reperfusion with technetium-99m methoxyisobutyl isonitrile. *Circulation* 1990;82:1424-1437.
30. Knabb RM, Bergmann SR, Fox KAA, et al. The temporal pattern of recovery of myocardial perfusion and metabolism delineated by positron emission tomography after coronary thrombolysis. *J Nucl Med* 1987;28:1563-1570.

Extracardiac Activity Complicates Quantitative Cardiac SPECT Imaging Using a Simultaneous Transmission-Emission Approach

Eliot N. Heller, Paul DeMan, Yi-Hwa Liu, Donald P. Dione, I. George Zubal, Frans J.T. Wackers and Albert J. Sinusas
Experimental Nuclear Cardiology Laboratory, Division of Cardiovascular Medicine, Department of Internal Medicine, and Department of Diagnostic Radiology, Yale University School of Medicine, New Haven, Connecticut

Increased extracardiac activity confounds conventional cardiac SPECT image reconstruction using a filtered backprojection method. Others have proposed that simultaneously acquired transmission-emission (STE) images that are reconstructed with a maximum likelihood (ML) method incorporating a nonuniform attenuation correction would less likely be affected by the presence of extracardiac activity. However, this approach corrects only for decreased myocardial counts from attenuation and not for increased myocardial counts from extracardiac activity. Therefore, STE with nonuniform attenuation correction may also result in reconstruction artifacts when extracardiac activity is present. **Methods:** Acquisitions of phantoms with nonuniform and uniform attenuation were performed using STE and conventional approaches, in the absence and presence of extracardiac activity. All acquisitions used a triple-headed SPECT camera. STE acquisitions used fanbeam collimation and a ¹⁵³Gd transmission source. STE images were reconstructed using ML, with and without nonuniform attenuation correction. Reconstructed short-axis images were quantitated, and percentage variability for each count profile was calculated. **Results:** In a nonuniform phantom configuration, STE reconstruction with nonuniform attenuation correction significantly improved image uniformity. This improvement in image uniformity

was diminished with the addition of increasing extracardiac activity. In a uniform phantom, STE reconstruction with nonuniform attenuation correction significantly improved uniformity only in the presence of extracardiac activity. **Conclusion:** The addition of attenuation correction in the presence of extracardiac activity can have complex effects on ML reconstruction with nonuniform attenuation correction, which depends on the amount of extracardiac activity and pattern of attenuation.

Key Words: attenuation correction; quantitative SPECT; artifacts; emission transmission

J Nucl Med 1997; 38:1882-1890

Extracardiac activity can artificially decrease or increase counts in the adjacent regions in the heart. A decrease in the intensity of the target organ (heart) has been attributed to the surrounding negative values (1,2) from the adjacent extratarget activity when conventional filtered backprojection image reconstruction is used (3). Alternatively, an increase in intensity can

Received Aug. 26, 1996; revision accepted Feb. 26, 1997.

For correspondence or reprints contact: Albert J. Sinusas, MD, Yale University School of Medicine, P.O. Box 208042, TE-2, New Haven, CT 06520-8042.

occur in the target organ as a result of the Compton scattering (3) from neighboring organs.

Maximum likelihood (ML) reconstruction has been proposed as a means for reducing artifacts associated with increased liver activity (1) because this method follows the positivity constraint. Consequently, the negative pixel values caused by the conventional method do not occur when the ML method is used. Nuyts et al. (4) found that extracardiac activity slows the convergence of ML reconstruction in the heart region. They proposed the addition of nonuniform attenuation correction to ML reconstruction for the reduction of artifacts caused by extracardiac activity.

Because scatter photons remain uncorrected, it was hypothesized that extracardiac activity could cause different and potentially more severe artifacts in SPECT images reconstructed using ML with attenuation correction. To test this hypothesis, the effects of extracardiac activity on simultaneously acquired transmission-emission (STE) images reconstructed with the ML method were compared with the effects on conventionally acquired SPECT images.

MATERIALS AND METHODS

The effect of increased extracardiac activity on cardiac SPECT image uniformity was evaluated by a series of phantom studies. First, a phantom configuration with nonuniform attenuation was used to simulate the human thorax, allowing the evaluation of the effects of extracardiac activity under normal conditions. After this initial study, a second phantom configuration with nearly uniform attenuation was evaluated to provide specific insight into the effects of variation in the distance of the extracardiac activity from the target organ, while minimizing the variation in attenuation. Both conventional and STE imaging approaches were applied for each phantom configuration. Simultaneously acquired transmission-emission images were reconstructed using a ML algorithm, both with and without the implementation of a nonuniform attenuation correction. All images were acquired and reconstructed using a commercially available system. There were differences in both the collimation and the reconstruction, depending on which imaging approach was applied, as dictated by the manufacturer.

Phantom Configurations

Nonuniform Phantom. A Data Spectrum Jaszczak heart in torso phantom was used that consisted of a cardiac insert in an elliptical chest. Lungs and Teflon spine (Data Spectrum, Chapel Hill, NC) were also inserted to simulate the nonuniform attenuation distribution in a patient. The liver was simulated by attaching a 1-liter intravenous bag to the inferior aspect of the right lung, approximately 1 cm from the inferior surface of the heart. The cardiac phantom was prepared with 500 μCi (18.5 MBq) of $^{99\text{m}}\text{Tc}$ in the myocardial space (1-cm-thick). The remaining spaces in the torso and the cardiac cavity were filled with water.

A total of eight SPECT acquisitions was completed imaging each of the four "liver"-to-"heart" ratios, conventionally and with STE. These liver-to-heart ratios were chosen to reflect the range of activities that might be observed clinically when imaging is performed with $^{99\text{m}}\text{Tc}$ -labeled myocardial perfusion tracers. Actual liver-to-heart maximum count ratios were determined from the conventional raw images by measuring regions of over the heart and the liver. The eight acquisitions were:

1. Conventional, 0:1 liver-to-heart ratio;
2. STE, 0:1 liver-to-heart ratio;
3. Conventional, 1:1 liver-to-heart ratio;
4. STE, 1:1 liver-to-heart ratio;
5. Conventional, 5:1 liver-to-heart ratio;
6. STE, 5:1 liver-to-heart ratio;

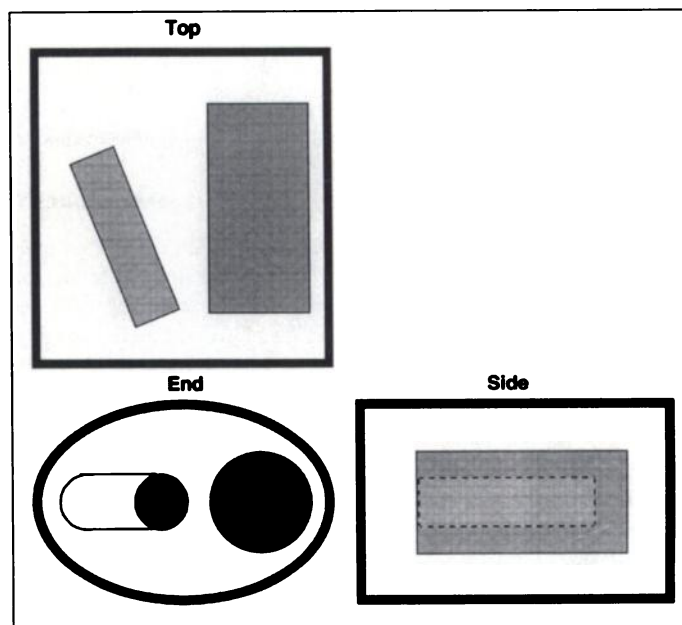


FIGURE 1. Schematic of the uniform phantom. The larger cylinder represents the target organ (heart), and the smaller cylinder represents the extracardiac source of scatter (liver).

7. Conventional, 10:1 liver-to-heart ratio; and
8. STE, 10:1 liver-to-heart ratio.

Uniform Phantom. To better define the effects of extracardiac activity on image uniformity, using each of the reconstruction approaches, a simplified phantom was evaluated. This phantom (Fig. 1) consisted of two cylinders in a Data Spectrum elliptical chest. The larger of the two cylinders represented the heart and was made up of concentric cylinders with a 1.5-cm-thick chamber, which was filled with radioactive water [500 μCi (18.5 MBq) of $^{99\text{m}}\text{Tc}$]. This cylinder was placed in the left side of the chest, parallel to the center of the camera orbit. A second smaller cylinder, which had only one chamber, was placed with its long axis at approximately a 30° angle from the heart cylinder. The center of the small cylinder was elevated to the level of the center of the larger cylinder. The elliptical chest phantom and larger cylinder cavity were filled with water to provide a uniform scatter medium. This phantom's only significant asymmetry was the eccentric placement of the larger cylinder in the left chest and will therefore be referred to as the "uniform" phantom hereafter.

Gadolinium has an energy of 98 keV, which falls into the energy range of the Compton scatter of $^{99\text{m}}\text{Tc}$. Therefore, down scatter from extracardiac structures could contaminate the transmission map used for the nonuniform attenuation correction. We postulated that by increasing the strength of the transmission source, we could reduce the effects of down scatter of the emission counts into the transmission window by reducing the relative percentage of down scatter counts into the transmission window. Therefore, STE acquisitions of the uniform phantom were each done twice: first, using a stronger filter in front of the Gd-153 transmission source, thus providing attenuation information from a relatively weaker transmission source (106 kcps); and second, using a thinner filter in front of the ^{153}Gd transmission source, thus providing attenuation information from a relatively stronger transmission source (122 kcps). Both levels of transmission activity were within the manufacturer's recommended range (90–140 kcps in calibration mode) for clinical imaging.

Six SPECT acquisitions were performed using the uniform phantom configuration. These acquisitions were:

1. Conventional without extracardiac activity;

2. STE without extracardiac activity, weak transmission source;
3. STE without extracardiac activity, strong transmission source;
4. Conventional with extracardiac activity;
5. STE with extracardiac activity, weak transmission source; and
6. STE with extracardiac activity, strong transmission source.

To determine the system's ideal uniformity, the larger cylinder was also imaged alone with no attenuating medium. These images were acquired using parallel-hole collimators, with the cylinder placed in the center of a circular orbit and reconstructed using a filtered backprojection reconstruction.

Image Acquisition

All acquisitions were performed using a triple-headed gamma camera system. Both conventional and STE images were acquired using continuous noncircular 20-min orbits.

Conventional. Conventional images were acquired using high-resolution, parallel-hole collimation, 120° rotation per head, 20 projections per head (60 sec per projection) and a magnification of 1.33.

Simultaneously Acquired Transmission-Emission. The STE approach for SPECT imaging differed from the conventional approach to SPECT imaging in several ways. Fanbeam collimators were used for the acquisition of both emission and transmission images. The STE images were acquired using 360° rotation per head, 40 projections per head (10 sec per projection) and a magnification of 1.0. When imaging was performed with a ^{99m}Tc-labeled radiotracer, a 60-mCi (2.2-GBq) ¹⁵³Gd collimated line source is used for the acquisition of the transmission images. The transmission and emission images were acquired simultaneously using two separate energy windows. We used a 20% window centered in the photopeak of each radiotracer (¹⁵³Gd, 98 keV; ^{99m}Tc, 140 keV). The transmission images were then used to construct a nonuniform attenuation map. The final images were then reconstructed using a modified STE algorithm with the attenuation map incorporated to provide a nonuniform attenuation correction.

Image Reconstruction

Conventional. The conventionally acquired images were reconstructed using the filtered backprojection method without prefiltering. Three-dimensional, low-pass postfiltering was applied to all conventional acquisitions. All transverse images were reoriented to generate 10 5-mm-thick short-axis images.

Simultaneously Acquired Transmission-Emission. The STE images were reconstructed using the ML algorithm. An off-center zoom was applied to increase the STE image size so that it was consistent with the size of the conventionally acquired images. Each STE reconstruction was done twice, once with and once without a nonuniform attenuation correction. Three-dimensional, low-pass postfiltering was applied to all images reconstructed using STE. Again, all transverse images were reoriented to generate 10 5-mm-thick short-axis images.

Due to software limitations, we were not able to reconstruct the conventional data using the ML algorithm, nor were we able to reconstruct STE data acquired with fanbeam collimators using filtered backprojection.

Quantitative Image Analysis

Ten reconstructed short-axis slices were interpolated to create 36 short-axis slices. Each slice was divided into 128 sectors, starting at 45° and then proceeding counterclockwise. The maximum count per sector was used to create a circumferential count profile for each slice (5). A flat, seven-point smoothing was applied to all sector values. The sector values for all 36 slices were then normalized to the sector with the highest intensity. Three-dimen-

TABLE 1
Variability of Nonuniform Phantom

Liver-to-heart ratio	Conventional	STE-ML	STE-ML and NAC
0:1	10.5 ± 1.2	9.9 ± 1.3	5.8 ± 1.9*
1:1	12.6 ± 3.5 [†]	10.1 ± 3.2	6.8 ± 2.6
5:1	14.1 ± 3.75 [†]	9.4 ± 3.1	7.0 ± 2.7 [‡]
10:1	18.8 ± 4.3 [†]	10.8 ± 3.3	12.2 ± 3.5 [‡]

*p < 0.001 when compared to STE-ML at same level of liver activity.

[†]p < 0.001 when compared to 0:1, conventional.

[‡]p < 0.001 when compared to 0:1, STE-ML and NAC.

NAC = nonuniform attenuation correction.

sional graphs were generated that displayed the globally normalized counts for each type of reconstruction.

The mean counts and s.d. were calculated for each of the 36 slices for each acquisition. Percentage count variability was computed for each slice by dividing the s.d. by the mean value and then multiplying by 100. In addition, for the uniform phantom, the 36 slices were separated into thirds (apical, midventricular and basal). Variabilities were computed for each portion and compared.

The variation in image resolution was evaluated for each of the different imaging approaches by performing linear count profiles through the uniform cardiac phantom (1-cm-thick) in the absence of extracardiac activity.

Statistical Analysis

Nonuniform Phantom. Short-axis image variabilities from each type of image reconstruction were compared at each liver-to-heart ratio. A single-factor ANOVA test with Bonferroni correction was used to test if the difference in variability between each reconstruction was significant.

Uniform Phantom. Short-axis image variability from each type of image reconstruction were compared with each other (with and without extracardiac activity) and the acquisition of the cylinder

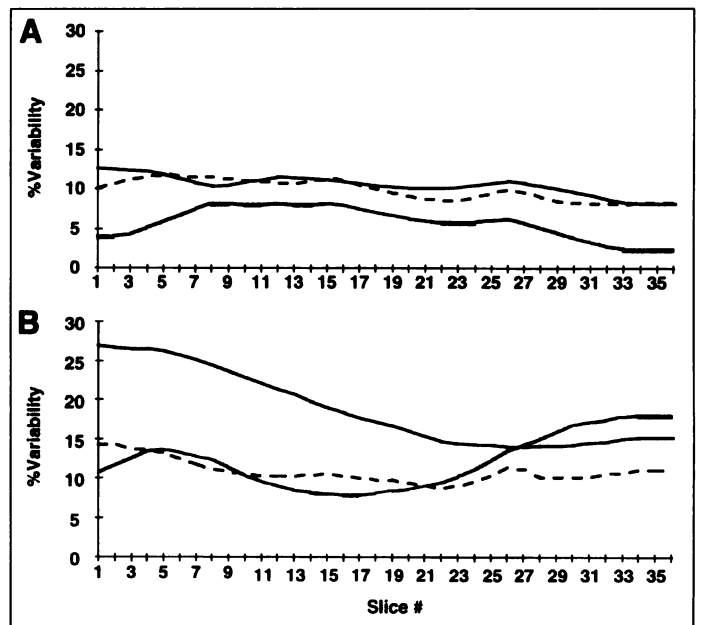


FIGURE 2. Nonuniform phantom. (A) Image variability with no extracardiac activity. The ML with attenuation correction has the least variability. (B) Image variability from the highest liver-to-heart ratio. The variability for the conventional reconstruction was highest towards the apex (slice 1), whereas for the ML reconstruction with nonuniform attenuation correction, it was highest towards the base. Solid black line, conventional; dashed line, ML without attenuation correction; solid gray line, ML with attenuation correction.

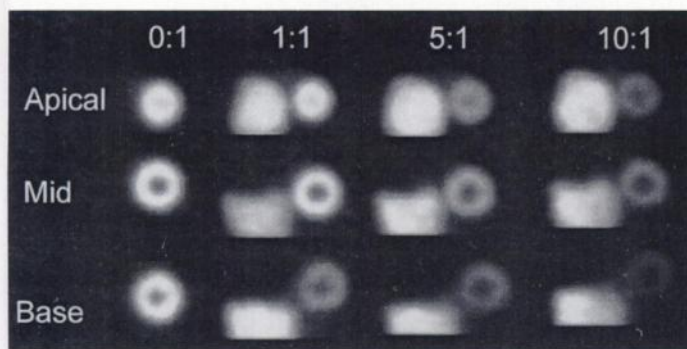


FIGURE 3. Nonuniform phantom with increasing extracardiac activity. Shown are short-axis slices from the nonuniform phantom reconstructed with ML implementing the nonuniform attenuation correction. Representative slices from apical, midventricular and basal levels are shown without liver activity and increasing levels of liver activity. The relative cardiac activity decreases with increasing liver activity. In addition, the cardiac activity decreases from apex to base with increasing depth within the phantom.

alone. A single-factor ANOVA test with Bonferroni correction was used to test if the difference in variability between each reconstruction was significant. Single-factor ANOVA was also used to compare the variability of each third of the larger cylinder.

RESULTS

Nonuniform Phantom

No Extracardiac Activity. The images of the nonuniform phantom reconstructed conventionally had decreased image intensity in the lower quadrant, most likely caused by attenuation by the imaging table. There was also increased intensity in the upper right quadrant, probably because the camera passed closest to this region. The images acquired with STE and reconstructed with ML without using nonuniform attenuation

correction were slightly more uniform, although they demonstrated a similar pattern. The addition of nonuniform attenuation correction changed the image pattern completely. The lower quadrant demonstrated the greatest image intensity, whereas the right and left quadrants demonstrated decreased image intensity. For all methods of reconstruction, image intensity gradually decreased, moving from apex to base.

Variabilities for each of the nonuniform phantom acquisitions are summarized in Table 1. Quantitative analysis confirmed that there was no significant difference between the variability using the conventional reconstruction or ML reconstruction without attenuation correction. The STE-ML approach with nonuniform attenuation correction provided significantly more uniform cardiac images in the phantom with nonuniform attenuation, when compared to the other methods, in the absence of extracardiac activity. Figure 2A shows that the variability for STE-ML with nonuniform attenuation correction was superior for all short-axis slices from apex to base.

Extracardiac Activity Present. In the presence of extracardiac activity, the lower left quadrant adjacent to the liver had less intensity in the images reconstructed using the conventional method. Increasing the liver-to-heart activity ratio did not further alter the visual appearance of the heart image using conventional acquisition parameters and filtered backprojection. However, there was an increase in image variability with increasing liver activity. Even the lowest levels of extracardiac activity (liver-to-heart ratio of 1:1) significantly changed the quantitative image profiles using the conventional approach. The variability was highest at the apex with the conventional reconstruction (Fig. 2B).

Application of ML reconstruction without attenuation correction unexpectedly improved image uniformity for all the liver-to-heart ratios (Table 1). Even at the highest levels of extracardiac activity (liver-to-heart ratio of 10:1), the variability was not

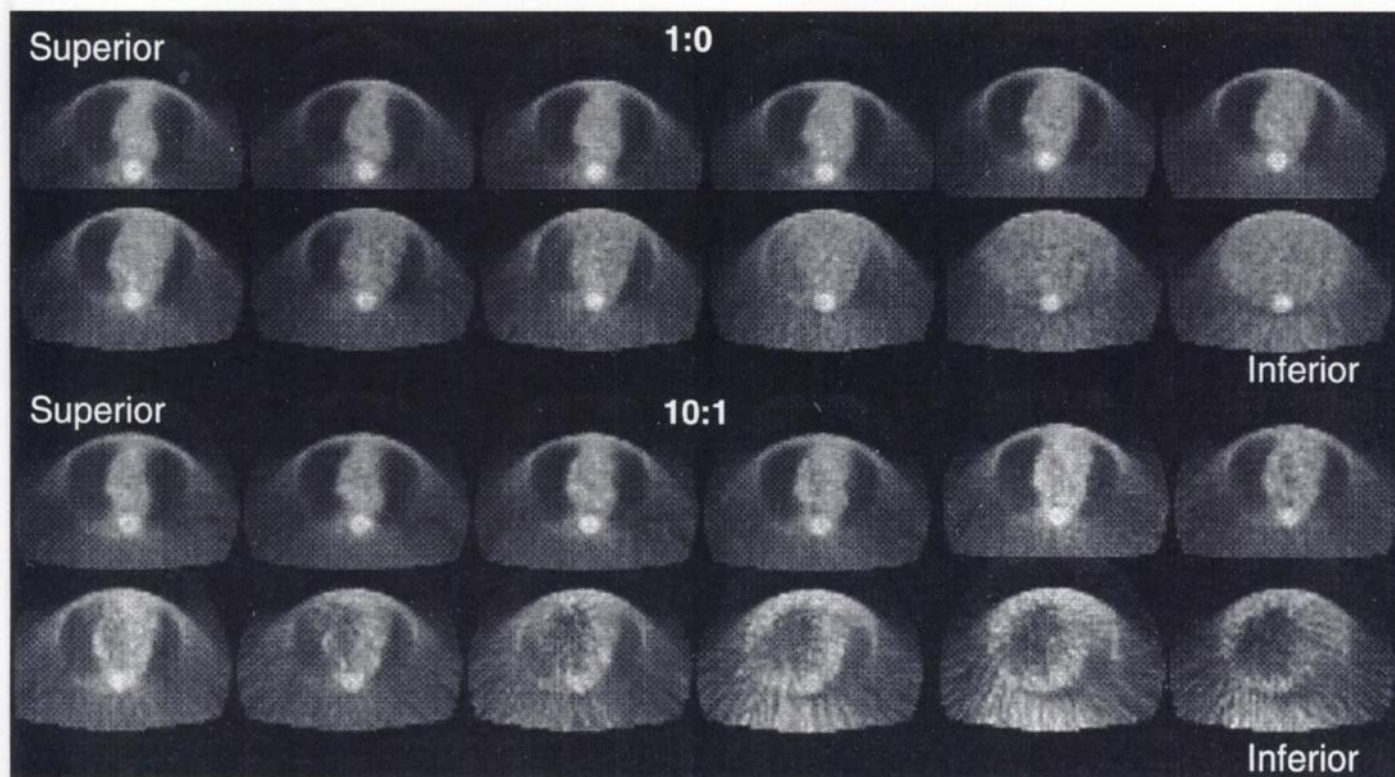
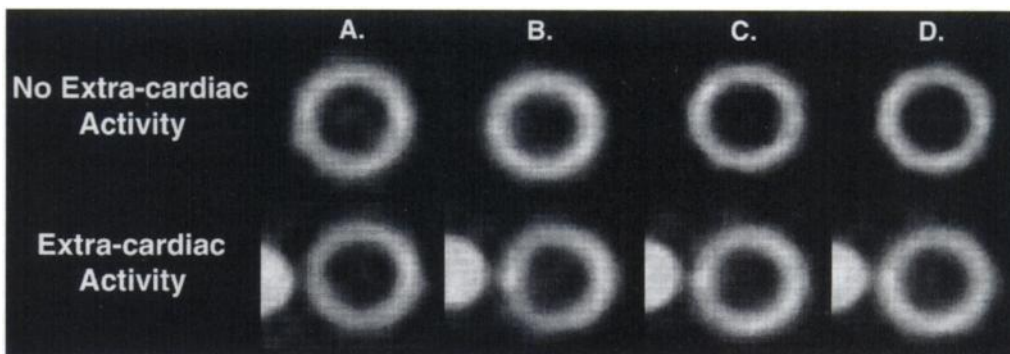


FIGURE 4. Transmission maps. (Upper) Transmission maps from the nonuniform phantom without liver activity. Images are displayed superior to inferior. (Lower) Transmission maps from the nonuniform phantom with liver-to-heart ratio of 10:1. Note the streaking and the loss of definition of the structures in the attenuation maps in the presence of increased liver activity.

FIGURE 5. Uniform phantom: short-axis images. Representative midventricular cylinder short-axis images are shown of the heart cylinder without (upper) and with (lower) activity in the liver cylinder. Images are acquired and reconstructed using one of four approaches: conventional (A), ML without attenuation correction (B) and ML reconstruction with nonuniform attenuation correction using a weaker (C) and a stronger (D) source. Note the addition of extracardiac activity results in a subtle decrease in activity in the lower left quadrant of the conventional reconstruction, increased activity in the left wall of the ML reconstruction without attenuation correction and improved image uniformity in both the ML reconstructions with attenuation correction.



significantly different then when no extracardiac activity was present (liver-to-heart ratio of 0:1).

The addition of nonuniform attenuation correction resulted in minimal image improvement. At the highest levels of liver-to-heart activity ratio (10:1), it became very difficult to visually interpret the heart images secondary to the confounding liver activity. Representative short-axis images from apical, midventricular and basal regions using the ML with nonuniform attenuation correction method for each of the liver-to-heart ratios are illustrated in Figure 3. Short-axis image intensity decreased with increasing extracardiac activity. Short-axis image intensity also decreased with increasing attenuation, as is typically seen at the base of the heart. Nevertheless, the advantage of nonuniform attenuation correction over just ML was lost when the liver-to-heart ratios was increased to the 5:1 level. At the highest levels of liver-to-heart ratios, the addition of nonuniform attenuation correction increased variability above that observed with ML without attenuation correction. The variability was highest at the base of the heart phantom (Fig. 2B).

To better understand the effect of extracardiac activity on the nonuniform phantom, the attenuation maps in the presence of 0:1 and 10:1 liver-to-heart ratios were compared (Fig. 4). These attenuation maps were derived from the transmission data. The maps generated in the absence of extracardiac activity clearly delineate the nonuniform structures. In contrast, the attenuation maps generated with the presence of the highest liver-to-heart ratio became very distorted and streaky, especially in the regions closest to the liver.

Uniform Phantom

No Attenuation. The large cylinder from the uniform phantom was first imaged in isolation using conventional SPECT acquisition and filtered backprojection reconstruction. Under these ideal conditions, there was excellent image uniformity. The variability in the circumferential count profile of the reconstructed short-axis images was $4.4\% \pm 0.4\%$. This value was considered ideal variability.

No Extracardiac Activity. Short-axis images of the uniform phantom (now in the torso phantom) were generated using four acquisition protocols. Images were compared both visually (Fig. 5) and quantitatively (Fig. 6). Of the four methods of reconstruction, the ML reconstruction without nonuniform attenuation correction provided the most uniform images with visual inspection.

Quantitative analysis of all the short-axis, three-dimensional count profiles confirmed our visual observations (Fig. 6). The image count profile variability from each of the uniform phantom acquisitions is summarized in Table 2. In the absence of extracardiac activity, the least variability was seen when ML was applied without nonuniform attenuation correction. The implementation of nonuniform attenuation correction (weaker source) resulted in significantly increased variability. The quantitative analysis also revealed that the increased activity in the lower quadrant observed with ML with nonuniform attenuation correction was more intense and discrete when the stronger transmission source was used. In the absence of extracardiac activity, the ML reconstruction without nonuniform attenuation correction provided the best quantitative image uniformity. In fact, ML reconstruction produced images that were even more uniform than the system ideal.

Linear count profiles through the uniform cardiac phantom were generated to evaluate changes in image resolution. These profiles were normalized to a region of the cardiac phantom closest to the surface of the elliptical chest, which would be anticipated to have the least attenuation (Fig. 7). These profiles showed there was less than a 1-pixel difference between the FWHM for any of the four approaches. Additionally, note that in the least attenuated wall (right peak), all approaches had similar intensities. However, in the most attenuated wall (left peak), the conventional and STE without attenuation correction had decreased intensity, whereas the STE using either the strong or the weak line source had greater intensity than the maximum.

TABLE 2
Variability of Uniform Phantom

Activity	Conventional	STE-ML	STE-ML and NAC, weaker source	STE-ML and NAC, stronger source
No extracardiac activity	7.6 ± 1.4	$3.0 \pm 0.6^*$	$9.1 \pm 0.5^*$	$10.4 \pm 0.4^{*†}$
Extracardiac activity	9.9 ± 0.8	$12.1 \pm 0.5^*$	$6.5 \pm 0.9^*$	$4.8 \pm 1.3^{*†}$

*p < 0.001 when compared to conventional at same level of liver activity.

†p < 0.001 when compared to ML with weaker source at same level of liver activity.

NAC = nonuniform attenuation correction.

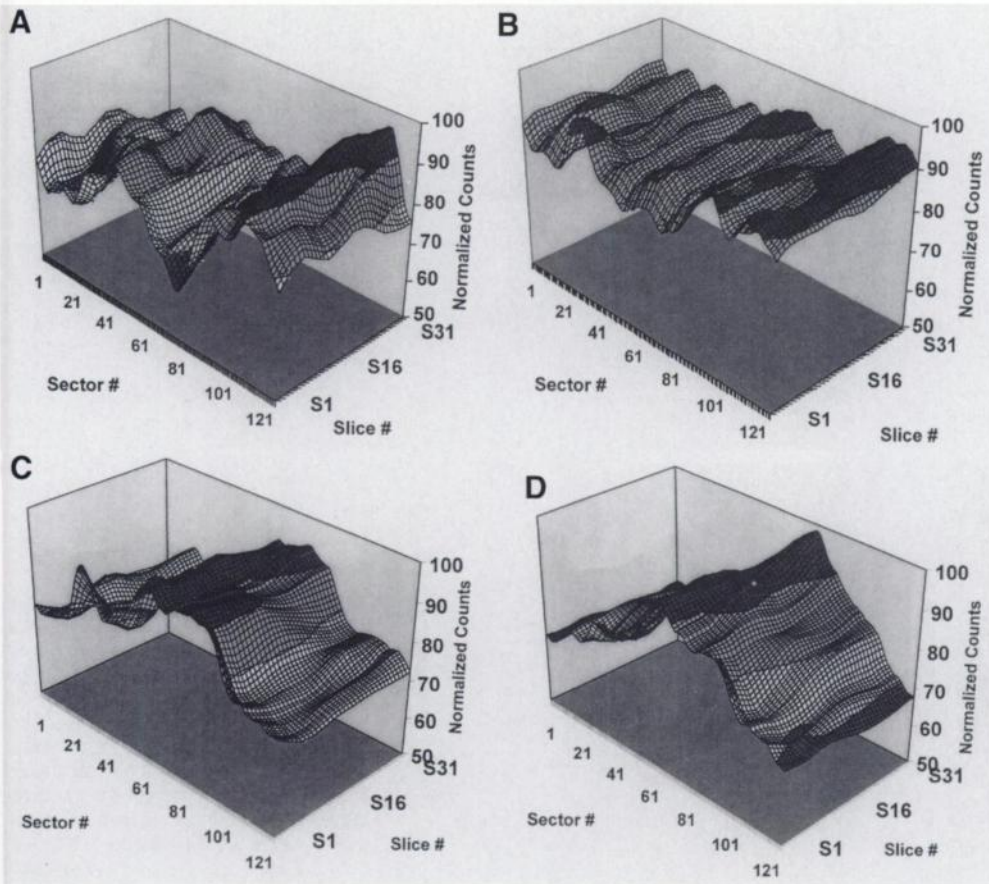


FIGURE 6. Uniform phantom without extracardiac activity; image quantitation. Normalized circumferential count profiles are shown for conventional (A), ML without attenuation correction (B) and STE-ML with the weaker (C) and stronger (D) line source. Note that the STE-ML without attenuation correction produces the most uniform images.

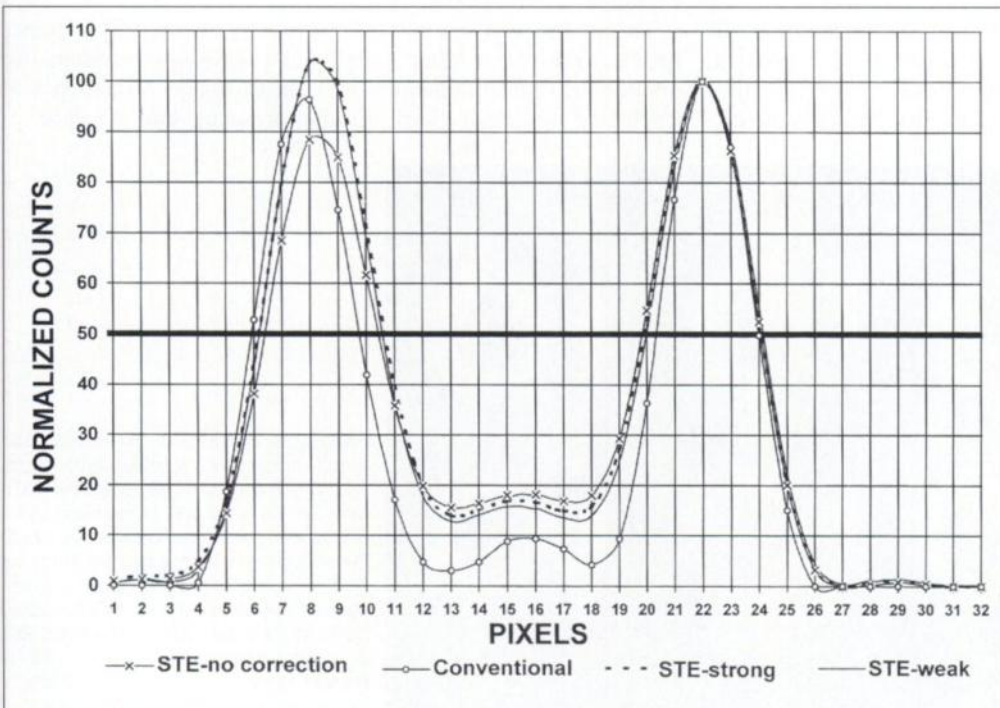


FIGURE 7. Linear count profiles through the uniform cardiac phantom. Normalized linear count profiles through the uniform cardiac phantom (wall thickness, 1 cm) are shown. Note that there was less than a 1-pixel difference of the FWHM for any of the approaches.

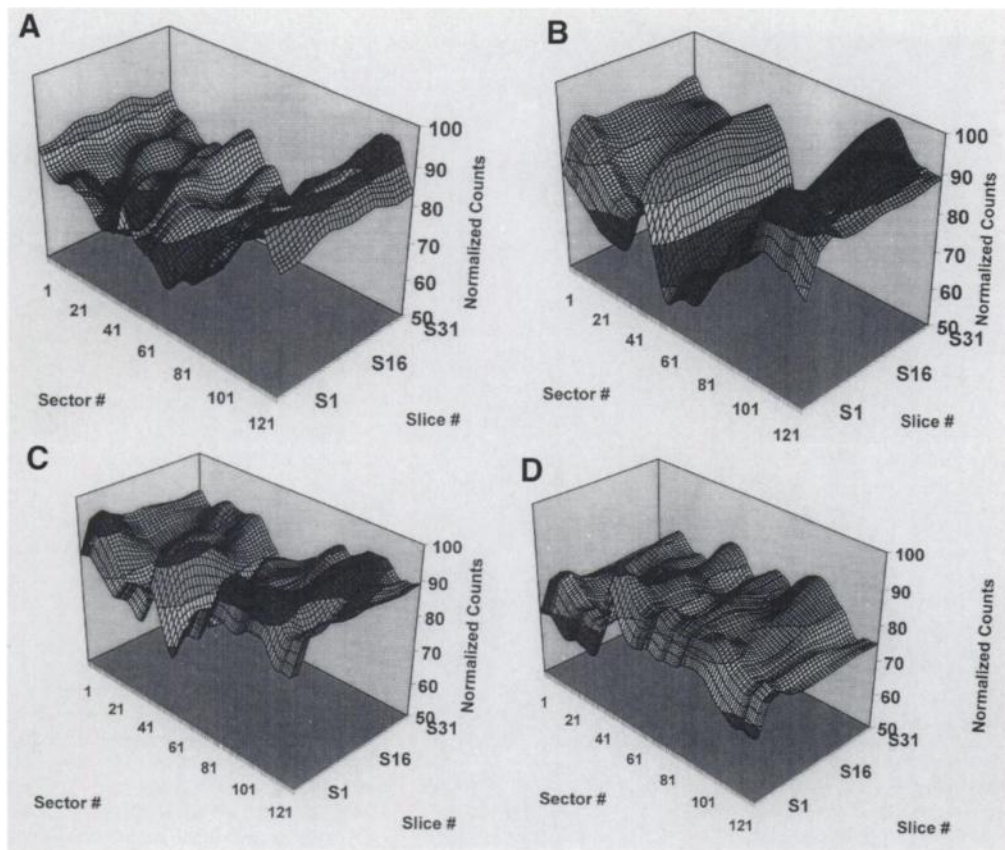


FIGURE 8. Uniform phantom with extracardiac activity: image quantitation. Normalized circumferential count profiles are shown for conventional (A), ML without attenuation correction (B) and STE-ML with the weaker (C) and stronger (D) line source. Note that STE-ML with attenuation correction provides the most uniform images. The strong transmission source provided some improvement in uniformity over the weaker source.

Extracardiac Activity Present. The overall image uniformity of the uniform phantom in the presence of extracardiac activity was also assessed for each reconstruction method, both visually and quantitatively (Figs. 5 and 8). Similar to the nonuniform phantom, conventional image reconstruction produced images with decreased intensity in the left quadrant, which was closest to the extracardiac activity (Fig. 5). Again, like the nonuniform phantom, the ML reconstruction without attenuation correction resulted in increased image intensity in the left quadrant. This increase in intensity persisted along the entire length of the cylinder despite the gradual increase in distance of the liver cylinder from the heart cylinder (Fig. 9). The addition of extracardiac activity resulted in a considerable increase in image variability of the uniform phantom using the ML reconstruction without nonuniform attenuation correction (Table 2).

The ML reconstruction with implementation of the nonuniform attenuation correction also resulted in increased intensity in the left quadrant of the short-axis slice. However, the increased intensity only involved the first few slices, where the extracardiac activity was closest to the cardiac phantom. The addition of nonuniform attenuation correction (weaker transmission source) significantly decreased variability of the STE acquisitions. The stronger transmission line source visually and quantitatively further improved the image uniformity.

Distance Comparison

To determine if image uniformity was affected by distance between the extracardiac activity and the heart phantom, we divided the uniform phantom into thirds. Image variability was calculated for each third, in the presence and absence of

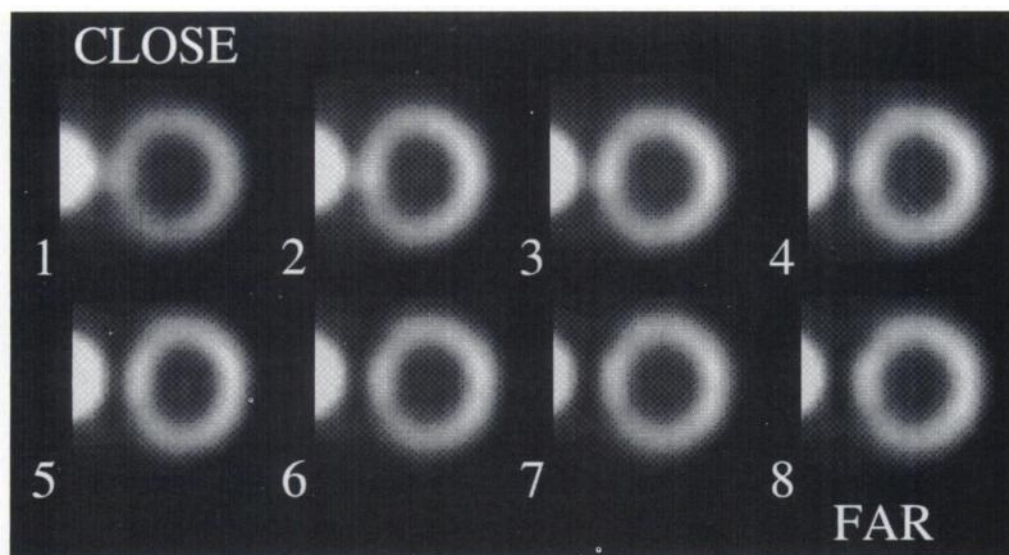


FIGURE 9. Distance of the extracardiac activity from heart affects ML reconstruction. These short-axis slices are the complete set from the end of the heart cylinder, which is closer, to the liver cylinder to the other end, which is farthest from the scatter source. Shown are short-axis images of the heart cylinder reconstructed using ML without attenuation correction. Increased intensity in the left wall is present in all slices, despite the increasing distance from the scatter source.

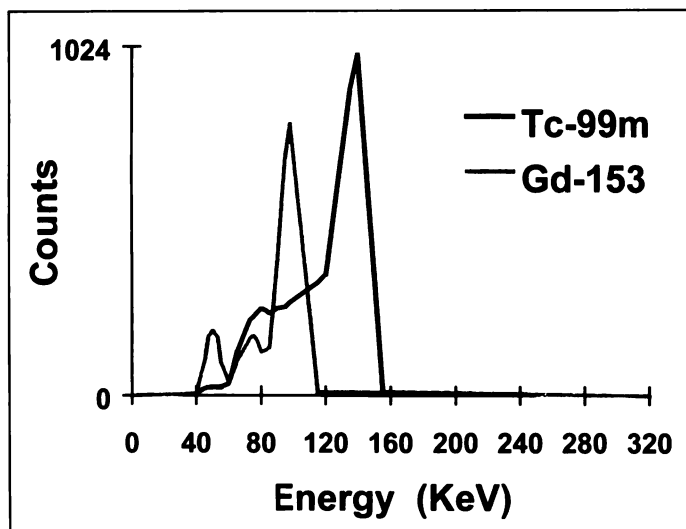


FIGURE 10. Energy spectra of the emission ^{99m}Tc counts and the transmission ^{153}Gd line source are superimposed. These spectra demonstrate the relative scatter down of ^{99m}Tc into the ^{153}Gd window.

extracardiac activity. With all the reconstruction methods, the change in variability in the presence of extracardiac activity did not vary significantly with the increase in distance from the extracardiac source.

DISCUSSION

The detrimental effects of extracardiac activity on the uniformity of standard conventional reconstruction of cardiac SPECT images have been previously detailed. Others had proposed that a ML approach with attenuation correction would improve the uniformity of cardiac SPECT images acquired in the presence of extracardiac activity. We hypothesized that extracardiac activity would cause other artifacts in SPECT images reconstructed using ML with attenuation correction because of residual uncorrected scatter. Accordingly, the effects of extracardiac activity on cardiac SPECT reconstruction were evaluated qualitatively and quantitatively with phantoms using standard conventional reconstruction and ML reconstruction, with and without nonuniform attenuation correction.

We evaluated a commercially available approach for nonuniform SPECT attenuation correction. This approach used fan-beam collimation and simultaneously acquired transmission images generated by using a ^{153}Gd transmission source opposing one of three camera heads.

Effects of Down Scatter

Our phantom studies suggest that down scatter into the transmission window causes a major problem for STE imaging using ^{99m}Tc -labeled perfusion tracers.

The experiments using the uniform phantom (uniform attenuation) without extracardiac activity demonstrated that the ML reconstruction without nonuniform attenuation correction resulted in the most uniform images. However, with the addition of extracardiac activity, application of ML reconstruction with nonuniform attenuation correction resulted in the best image uniformity. Additionally, the stronger transmission source further improved the final uniformity of the images of the uniform phantom in the presence of extracardiac activity.

Without extracardiac activity present, the more complex nonuniform phantom (nonuniform attenuation) had the most improved image uniformity when reconstructed using ML with nonuniform attenuation correction. The advantage of nonuniform attenuation correction was lost when extracardiac activity reached the 5:1 level. At the highest levels of liver-to-heart ratios, the

addition of nonuniform attenuation correction increased variability above that observed with ML without attenuation correction.

Review of the transmission maps (Fig. 3) revealed a striking distortion of the attenuation pattern. This may best be explained by inadequate correction for the down scatter or "cross talk" of ^{99m}Tc (140 keV) into the ^{153}Gd (98 keV) transmission window. Figure 10 is a graph that illustrates the potential mechanism for how increased liver intensity might distort the transmission maps. There should be an increase Compton scatter into the ^{153}Gd energy window in proportion to the increase in ^{99m}Tc activity in the liver. The down-scattered energy seen in the transmission window results in a decrease in attenuation being appreciated by the reconstruction process. This leads to significant under correction of attenuation from extracardiac structures with increased ^{99m}Tc activity (i.e., liver).

The other commercially available systems that perform attenuation correction also depend on the simultaneous acquisition of transmission and emission data. These systems will also be subject to the same distortions of down scatter into the transmission window when a transmission source that is of a lower energy than the emission isotope is used.

Effects of Distance

In our uniform phantom, varying the distance of extracardiac activity from our target organ resulted in no consistent alteration in image variability, regardless of the method used for reconstruction. This result suggests that these small changes in distance have relatively minimal effect on intensity of the scatter created by an extracardiac source.

However, the nonuniform phantom demonstrates that the STE approach to attenuation correction may be more affected by the magnitude of the attenuation correction required to produce the final image. For example, the closer the target organ is to the camera, the less the attenuation correction is a factor in the final image. Nevertheless, as the target organ moves deeper into the chest and further away from the camera, the final image becomes more dependent on the amount of attenuation correction that is applied, i.e., the more susceptible the image becomes to the distortion from the down scatter from an extratarget source. This was best demonstrated in the nonuniform phantom, in which the basal slices, which were deepest in the chest phantom, were more distorted by the increased liver intensity (Fig. 2). Therefore, the degree of attenuation correction required plays a much bigger role in the final cardiac image uniformity than does the distance of an extracardiac source from the heart.

Reconstruction Methods

The desire to correct for the artifacts caused by target organ attenuation has led to the development of simultaneous acquisition of emission and transmission data.

The use of a transmission source of a lower energy than that of the energy of the emission isotope was described by Bailey et al. (6). This initial study demonstrated that similar attenuation coefficients could be determined using a ^{153}Gd line source as with a ^{99m}Tc line source. They also demonstrated, in a small number of patients, that scatter from the emission ^{99m}Tc -labeled red blood cells into the ^{153}Gd window could be corrected to within 5% when attenuation correction was determined. However, the STE approach does not account for scatter into the transmission window from the emission isotope.

This study defines the problems associated with imaging a heart with intense adjacent liver activity. The implementation of the ML algorithm for reconstruction did improve image uniformity compared to filtered backprojection, as proposed by Germano et al. (1). Further improvement with the implementa-

tion of nonuniform attenuation correction was appreciated in the uniform phantom. In the nonuniform phantom, where there was nonuniform attenuation, the nonuniform attenuation correction improved image uniformity when there was no or minimal extracardiac activity.

Uniformity can easily be improved at the cost of decreased resolution. Although this study was not specifically designed to compare resolution, the linear count profiles of each approach to acquisition and reconstruction demonstrated no dramatic difference. These same profiles also demonstrated that this implementation of attenuation correction may over correct as shown by the increased counts of the left peak in Figure 7.

Additionally, the results of the uniform phantom acquisition without using attenuation correction demonstrated one of the previously described artifacts created by ML reconstruction. The increased activity in the adjoining scatter source can result in slowed convergence (4) in the target organ. This probably explains the resulting area of increased intensity along the whole length of the cylinder (Fig. 9).

Clinical Relevance

The findings of these experiments are important clinically because the ^{99m}Tc perfusion agents, like ^{99m}Tc -sestamibi, are eliminated primarily through the hepatobiliary system (7). Therefore, cardiac SPECT imaging is often complicated by extracardiac uptake. This can be an especially difficult problem when pharmacological stress agents such as adenosine (8) are used because of intense liver uptake associated with this form of cardiac stress. The presence of extracardiac uptake in the liver or bowel has previously been shown to confound the interpretation of cardiac SPECT images reconstructed with the conventional filtered-backprojection method (8). The current study suggests that extracardiac uptake also significantly impacts on iterative approaches for reconstruction, particularly if nonuniform attenuation correction is used with a transmission source.

CONCLUSION

The addition of attenuation correction in the presence of extracardiac activity can have complex effects on the final image appearance and quantitative analysis, depending on severity of attenuation and the amount of extracardiac activity present. If ML with nonuniform attenuation correction is to be applied to clinical cardiac SPECT imaging, then these confounding factors must be considered when interpreting qualitative and quantitative results.

Better SPECT attenuation correction may be obtained in the future by modifying existing approaches. One approach would involve acquisition of a transmission scan before the injection of the radiotracer and then performing a second transmission scan simultaneously with the emission acquisition. This approach would provide an uncontaminated attenuation map. The second transmission scan could then be used for registration of the uncontaminated first transmission scan and the emission data.

Alternatively, the transmission source strength could be varied so that a stronger transmission source is used in larger patients with more attenuation or in patients with poor clearance of activity from liver. Our experiments using an increased transmission source strength were a first step in testing this hypothesis.

Another approach would be the application of scatter correction algorithms, which would compensate for ^{99m}Tc down scatter. King et al. (2) used a Monte Carlo simulation to investigate cardiac SPECT artifacts caused by liver uptake. These authors concluded that the correction of both attenuation and scatter may overcome count gains and losses associated with hepatic activity (2).

Finally, the use of a transmission source with higher energy than the emission energy could provide improved attenuation maps. However, acquisition of emission data simultaneously with a high-energy transmission source may result in distortion of emission data due to down scatter from the transmission source.

All of these approaches could potentially help remove the effects of extracardiac activity. However, further testing is warranted before widespread application of simultaneous transmission-emission scanning can be recommended.

ACKNOWLEDGMENTS

This work was presented in part at the 42nd Annual Meeting of the Society of Nuclear Medicine, held June 12–15 1995, Minneapolis, MN. This research was supported in part by a grant from Picker International.

Dr. Heller was supported by a fellowship grant from the Connecticut affiliate of the American Heart Association. The project was also supported in part by a grant-in-aid from the American Heart Association.

REFERENCES

1. Germano G, Chua T, Kiat H, Areeda J, Berman D. A quantitative phantom analysis of artifacts due to hepatic activity in technetium-99m myocardial perfusion SPECT studies. *J Nucl Med* 1994;35:356–359.
2. King M, Xia W, deVries D, et al. A Monte Carlo investigation of artifacts caused by liver uptake in single-photon emission computed tomography perfusion imaging with technetium 99m-labeled agents. *J Nucl Cardiol* 1996;3:18–29.
3. Sorenson J, Phelps M. *Physics in nuclear medicine*. Philadelphia: W.B. Saunders; 1987:180–182, 394–401.
4. Nuyts J, Dupont P, Van den Maegdenbergh V, Vleugels S, Suetens P, Mortelmans L. A study of the liver-heart artifact in emission tomography. *J Nucl Med* 1995;36:133–139.
5. Liu YH, Sinusas AJ, Shi CQX, et al. An automated approach for quantification of relative regional myocardial blood flow, using SPECT Tc99m-sestamibi: preliminary validation in a canine model. In: Sheppard NF Jr., Eden M, Kantor G, eds. *Proceedings to the 16th annual international conference of the IEEE engineering in medicine and biology society*, Baltimore, MD, November 3–6: vol. 16. 1994:636–638.
6. Bailey D, Hutton B, Walker P. Improved SPECT using simultaneous emission and transmission tomography. *J Nucl Med* 1987;28:844–851.
7. Wackers F, Berman D, Maddahi J, et al. Technetium-99m hexakis 2-methoxyisobutyl isonitrile: human biodistribution, dosimetry, safety and preliminary comparison to thallium-201. *J Nucl Med* 1989;30:301–311.
8. Chua T, Kiat H, Germano G, et al. Rapid back to back adenosine stress/rest technetium-99m teboroxime myocardial perfusion SPECT using a triple detector. *J Nucl Med* 1993;34:1485–1493.